Linking rapid magma reservoir assembly and eruption trigger mechanisms at evolved Yellowstone-type supervolcanoes

Jörn-Frederik Wotzlaw[1]*, Ilya N. Bindeman[2], Kathryn E. Watts[3], Axel K. Schmitt[4], Luca Caricchi[1], and Urs Schaltegger[1]
[1]Section of Earth and Environmental Sciences, University of Geneva, 1205 Geneva, Switzerland
[2]Department of Geological Sciences, University of Oregon, Eugene, Oregon 97403, USA
[3]U.S. Geological Survey, 345 Middlefield Road, Menlo Park, California 94025, USA
[4]Department of Earth and Space Sciences, University of California–Los Angeles, Los Angeles, California 90095, USA

ABSTRACT

The geological record contains evidence of volcanic eruptions that were as much as two orders of magnitude larger than the most voluminous eruption experienced by modern civilizations, the A.D. 1815 Tambora (Indonesia) eruption. Perhaps nowhere on Earth are deposits of such supereruptions more prominent than in the Snake River Plain–Yellowstone Plateau (SRP-YP) volcanic province (northwest United States). While magmatic activity at Yellowstone is still ongoing, the Heise volcanic field in eastern Idaho represents the youngest complete caldera cycle in the SRP-YP, and thus is particularly instructive for current and future volcanic activity at Yellowstone. The Heise caldera cycle culminated 4.5 Ma ago in the eruption of the ~1800 km^3 Kilgore Tuff. Accessory zircons in the Kilgore Tuff display significant intercrystalline and intracrystalline oxygen isotopic heterogeneity, and the vast majority are ^{18}O depleted. This suggests that zircons crystallized from isotopically distinct magma batches that were generated by remelting of subcaldera silicic rocks previously altered by low-δ^{18}O meteoric-hydrothermal fluids. Prior to eruption these magma batches were assembled and homogenized into a single voluminous reservoir. U-Pb geochronology of isotopically diverse zircons using chemical abrasion–isotope dilution–thermal ionization mass spectrometry yielded indistinguishable crystallization ages with a weighted mean ^{206}Pb/^{238}U date of 4.4876 ± 0.0023 Ma (MSWD = 1.5; n = 24). These zircon crystallization ages are also indistinguishable from the sanidine ^{40}Ar/^{39}Ar dates, and thus zircons crystallized close to eruption. This requires that shallow crustal melting, assembly of isolated batches into a supervolcanic magma reservoir, homogenization, and eruption occurred extremely rapidly, within the resolution of our geochronology (10^3–10^4 yr). The crystal-scale image of the reservoir configuration, with several isolated magma batches, is very similar to the reservoir configurations inferred from seismic data at active supervolcanoes. The connection of magma batches vertically distributed over several kilometers in the upper crust would cause a substantial increase of buoyancy overpressure, providing an eruption trigger mechanism that is the direct consequence of the reservoir assembly process.

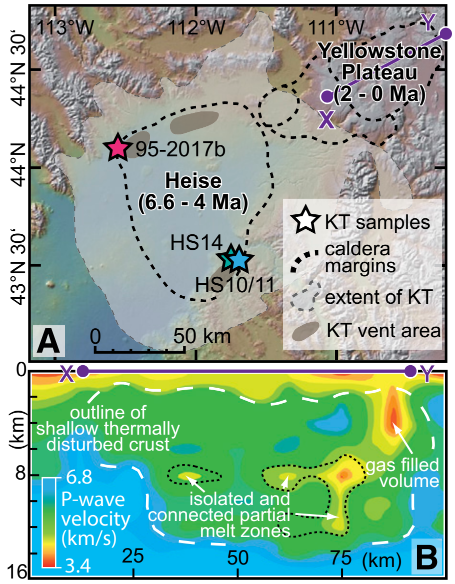

Figure 1. A: Digital elevation model showing mapped caldera margins of Heise and Yellowstone Plateau volcanic fields, inferred vent areas from which the Kilgore Tuff (KT) erupted, extent of related deposits (Morgan and McIntosh, 2005), and sample localities for samples analyzed in this study. X-Y line refers to subsurface interpretive cross section shown in B. B: Interpretive cross section through present-day Yellowstone subcaldera crust based on seismic P-wave velocities (modified from Miller and Smith, 1999) illustrating complex configurations of supervolcano magma reservoirs. Note that Husen et al. (2004) interpreted seismic data from Yellowstone to indicate a single connected reservoir, whereas two subreservoirs were well resolved beneath Toba (Indonesia; Stankiewicz et al., 2010).

INTRODUCTION

Supereruptions are among the most devastating natural disasters, and are more frequent than other extreme events of similar energy yield, such as meteorite impacts (Mason et al., 2004). During such eruptions hundreds to thousands of cubic kilometers of pyroclastic material are released within several days (Wilson and Hildreth, 1997), causing devastation on a regional scale by pyroclastic flows and ash falls, while released volcanic gases affect Earth's radiation budget, atmospheric circulation patterns, cause stratospheric ozone depletion, and ultimately global climate perturbations (Self and Blake, 2008). Understanding the time scales and mechanisms of assembly and storage of the magma reservoirs that feed supereruptions, as well as the mechanisms that trigger such eruptions, is important for assessing the probability and risk of future eruptions at active supervolcanoes (Lowenstern et al., 2006). Seismic tomography of large active systems of the Yellowstone (northwest United States) and Toba (Indonesia) supervolcanoes reveals complex spatial configurations of subcaldera low-velocity zones, interpreted as isolated or connected magma chambers (Miller and Smith, 1999; Husen et al., 2004; Stankiewicz et al., 2010; Fig. 1). Similar reservoir configurations have been inferred from chemical and isotopic diversity in the crystal cargo of ancient eruptive products at several volcanic provinces (e.g., Shane et al., 2008; Cooper et al., 2012; Ellis et al., 2014). However, the time scales over which such complex reservoirs are constructed and how long they are stable in the upper crust remains highly debated.

Here we take advantage of recent developments in high-precision U-Pb geochronology by isotope dilution–thermal ionization mass spectrometry (ID-TIMS) that allow dating of accessory zircon with uncertainties at the 0.1% level. This translates into absolute uncertainties of several thousand years for young volcanic units, providing insights into the time scales of magma chamber processes preceding eruptions (Crowley et al., 2007; Wotzlaw et al., 2013; Rivera et al., 2013). We combine this technique with in situ (secondary ion mass spectrometry, SIMS) oxygen and bulk crystal hafnium isotope analyses of the same zircon crystals. These data enable us to trace the origins of zircons and link their crystallization ages to the processes of rapid shallow magma segregation and batch assembly that led to eruption of one of the largest ignimbrite units on Earth, the Kilgore Tuff of the Heise volcanic field in eastern Idaho (western USA).

GEOLOGIC SETTING AND PREVIOUS MODELS OF SHALLOW MAGMA GENESIS IN THE SNAKE RIVER PLAIN

The Heise volcanic field is a nested caldera complex in the Snake River Plain–Yellow-

*E-mail: joern.wotzlaw@unige.ch.

GEOLOGY, September 2014; v. 42; no. 9; p. 807–810; Data Repository item 2014292 | doi:10.1130/G35979.1 | Published online 21 July 2014

stone Plateau (SRP-YP) volcanic province in eastern Idaho. The SPR-YP is the manifestation of interaction of plume-derived magmas with the overriding North American continent (e.g., Pierce and Morgan, 2009; Schmandt et al., 2012), generating large-scale crustal melting and a time-progressive sequence of caldera-forming eruptions. An important feature of SRP-YP volcanism is the abundance (~10,000 km^3 cumulative volume; e.g., Watts et al., 2011) of ^{18}O-depleted (i.e., low-δ^{18}O) eruptive products. These ignimbrites and lavas often contain populations of zircon with diverse δ^{18}O values, suggesting shallow crustal magma genesis by remelting of buried hydrothermally altered tuffs and their subvolcanic equivalents from previous eruptive cycles (e.g., Bindeman and Valley, 2001; Bindeman et al., 2007, 2008; Watts et al., 2011; Drew et al., 2013). The Yellowstone, Heise, and Picabo volcanic fields exhibit progressively lower δ^{18}O values of eruptive products and greater diversity in δ^{18}O of their zircon populations through time, indicating that remelting of hydrothermally altered low-δ^{18}O intracaldera material becomes progressively more important toward the end of caldera cluster evolution (Bindeman et al., 2008; Watts et al., 2011; Drew et al., 2013). Cannibalization of buried tuffs is particularly energy efficient, and numerical models suggest relatively short time scales (10^3–10^4 yr) for melting, assembly, and homogenization of high-temperature rhyolites in nested caldera settings (Simakin and Bindeman, 2012).

The Kilgore Tuff, the fourth, final, and most voluminous eruption in the Heise volcanic field, may be an analogue for current and future magmatic activity at Yellowstone. The young age of the Kilgore Tuff (ca. 4.5 Ma; Morgan and McIntosh, 2005) and the oxygen isotopic diversity of its zircon population (Watts et al., 2011) provide an ideal opportunity to quantify the time scales of the batch assembly process and homogenization of shallow magma reservoirs prior to eruption by employing high-precision chemical abrasion (CA) ID-TIMS U-Pb geochronology to these isotopically diverse zircons (Figs. 2 and 3).

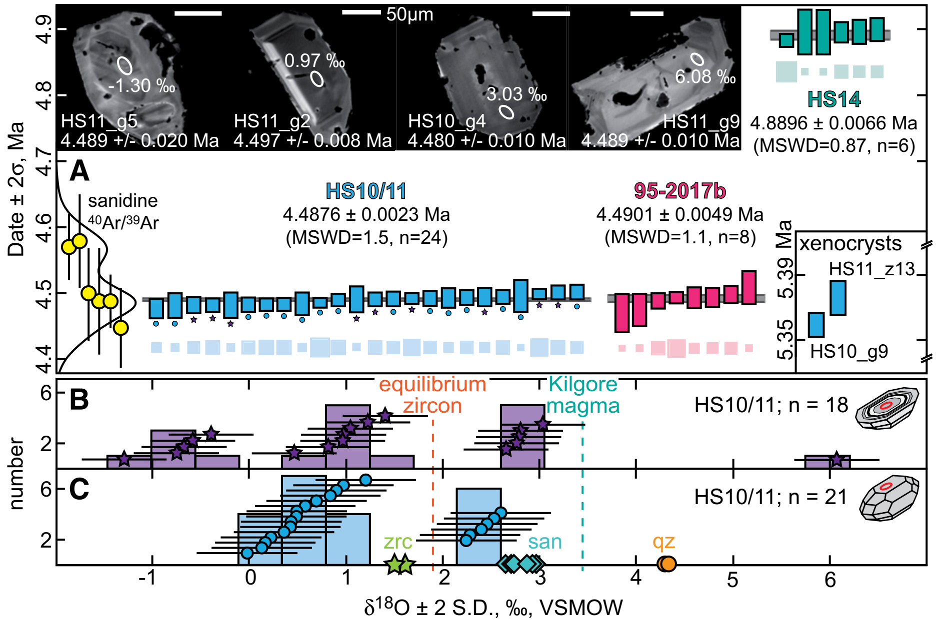

Figure 2. Oxygen isotope geochemistry and isotope dilution–thermal ionization mass spectrometry (ID-TIMS) U-Pb geochronology of Kilgore Tuff zircons. A: Ranked ^{206}Pb/^{238}U zircon dates corrected for initial ^{230}Th disequilibrium with 2σ analytical uncertainties. Horizontal bars are weighted mean dates; shaded squares below individual dates display their relative weights. Small symbols below dates of HS10/11 mark zircons that were analyzed for oxygen isotopes prior to ID-TIMS and refer to symbols in B and C. Also shown are sanidine ^{40}Ar/^{39}Ar dates for various Kilgore Tuff samples (Morgan and McIntosh, 2005) recalculated using calibration of Kuiper et al. (2008). MSWD—mean square of weighted deviates. Top: Cathodolumiscence images of selected zircons with locations of ion microprobe spots. B: Ion microprobe oxygen isotope data for zircon cores shown as histograms and individual data points with 2 standard deviation (S.D.) uncertainties. C: Ion microprobe oxygen isotope data for outermost zircon crystal faces. Also shown are the oxygen isotopic compositions of Kilgore Tuff sanidine (san), quartz (qz), and bulk zircon (zrc) fractions (Watts et al., 2011). VSMOW—Vienna standard mean ocean water.

ZIRCON OXYGEN ISOTOPE GEOCHEMISTRY

Interior domains of zircon crystals analyzed by SIMS are remarkably diverse with respect to their oxygen isotopic composition (Watts et al., 2011; Fig. 2; Table DR1 in the GSA Data Repository[1]). Individual spot analyses of exposed zircon cores range in $\delta^{18}O_{VSMOW}$ (Vienna standard mean ocean water) from –1.30‰ to +6.07‰ and can be grouped into at least 4 distinct populations (Fig. 2; Fig. DR1 in the Data Repository), suggesting that zircon cores crystallized from various isolated and isotopically distinct magma batches. Analyses of outermost zircon crystal faces yielded less isotopic diversity with two distinct populations (Fig. 2), recording progressive mixing of magmas from distinct batches during zircon crystallization.

These oxygen isotopic heterogeneities suggest that during reservoir assembly, several isotopically distinct subchambers coexisted in the subcaldera storage region (Fig. 3), resulting in a pre-eruption Kilgore magma reservoir configuration that resembles the reservoir configuration inferred from seismic data beneath Yellowstone and Toba (Miller and Smith, 1999; Husen et al., 2004; Stankiewicz et al., 2010; Figs. 1 and 3).

Notably, none of the analyzed zircon interior domains or the outermost zircon rims is in high-temperature isotopic equilibrium with sanidine and quartz that reflect the isotopic composition of the erupted magma ($\delta^{18}O_{magma}$ = +3.5‰; Fig. 2). This indicates that the time between final assembly and eruption was too short to isotopically equilibrate zircon rims diffusively, but long enough to equilibrate quartz and sanidine, providing independent mineral diffusive time scales for the time interval between assembly and eruption of hundreds to thousands of years (e.g., Bindeman et al., 2008). The lack of equilibrium crystal rims is consistent with zircon crystal size distributions (Fig. DR4). The observed deficit in small (~20–60 µm) crystals reflects crystal dissolution, suggesting that the Kilgore magma was zircon undersaturated for some time after final assembly of the reservoir. However, zircon crystal size distributions also show an excess in very small (~10 µm) crystals, suggesting renewed saturation, nucleation, and growth of zircon microlites just before eruption. Assuming constant growth rates of 10^{-14} to 10^{-15} cm/s, we estimate the time scale of zircon microlite crystallization to be 1.3–13 k.y. (for details, see Bindeman and Valley, 2001; Fig. DR4), consistent with mineral diffusive time scales derived from oxygen isotope disequilibria.

ZIRCON U-Pb GEOCHRONOLOGY AND THE TEMPO OF RESERVOIR ASSEMBLY

To quantify the time scales of shallow crustal reservoir assembly, we dated zircons with diverse oxygen isotopic compositions using CA-ID-TIMS techniques at the University of Geneva (for details, see the Data Repository). We analyzed a

[1]GSA Data Repository item 2014292, analytical details, additional figures and data tables, is available online at www.geosociety.org/pubs/ft2014.htm, or on request from editing@geosociety.org or Documents Secretary, GSA, P.O. Box 9140, Boulder, CO 80301, USA.

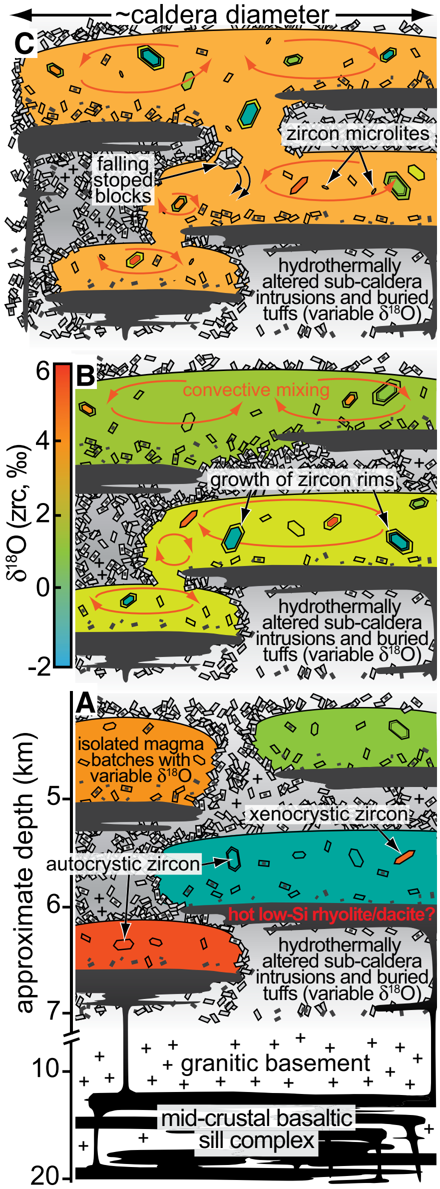

Figure 3. Illustration of the assembly process of the Kilgore Tuff magma reservoir and the origins of isotopically diverse zircons. A: Isolated isotopically distinct magma batches are generated by remelting of variably hydrothermally altered (variable δ^{18}O) subcaldera intrusions and buried tuffs. We envision that remelting is triggered by intrusion of hot, dry differentiates (low-Si rhyolites or dacites) that were generated by differentiation and crustal melting associated with a middle crustal basaltic sill complex, similar to that inferred from seismic data by Peng and Humphreys (1998). B, C: Progressive amalgamation of magma batches by thermal erosion/reactive bulk assimilation and/or mechanical failure of intrareservoir crust and convective homogenization prior to eruption. Colors of magma batches refer to equilibrium zircon oxygen isotopic composition. Crystals of same color as host magma are in oxygen isotopic equilibrium. Note increasing zircon (zrc) oxygen isotopic diversity with progressive assembly while other phenocrysts equilibrate. Alternatively, oxygen isotopic variability in zircons is the result of meter-scale heterogeneities, and small magma batches already had diverse zircon populations. Vertical exaggeration is ~1:10.

total of 34 zircons from densely welded, crystal-poor Kilgore Tuff from the southern (sample HS10/11; previously analyzed for oxygen isotopes) and northern (sample 95–2017b) outflow sheets, and 6 zircons from the pre–Kilgore Tuff ash-fall deposit (sample HS14; Figs. 1 and 2; Table DR2). After correction for ^{230}Th disequilibria (for details, see the Data Repository) single crystal ^{206}Pb/^{238}U dates of Kilgore zircons have an average 2σ uncertainty of 0.015 Ma that is 45 times more precise than previous ion microprobe U-Pb dates (Watts et al., 2011; Fig. DR2), allowing us to place much tighter constraints on the duration of reservoir assembly. Analyses (n = 24) of isotopically diverse zircons from the southern Kilgore outflow sheet yielded indistinguishable Th-corrected ^{206}Pb/^{238}U dates with uncertainties between 7 and 24 k.y. and a weighted mean of 4.4876 ± 0.0023 Ma (2σ; mean square of weighted deviates, MSWD = 1.5; Fig. 2). Eight U-Pb analyses of zircons from sample 95-2017b collected 80 km northwest (Fig. 1) yielded an indistinguishable weighted mean of 4.4901 ± 0.0049 Ma (MSWD = 1.1; Fig. 2). Pre–Kilgore Tuff zircons yielded a weighted mean ^{206}Pb/^{238}U date of 4.8896 ± 0.0066 Ma (MSWD = 0.87), i.e., ~400 k.y. older than the Kilgore Tuff zircons, suggesting that the two eruptions are unrelated and did not tap a common magma reservoir. The high precision of individual dates and the excellent reproducibility, despite large variations in δ^{18}O as well as zircon textural differences with variable proportions of textural features (e.g., resorbed interior domains; Fig. DR1), suggest that the age differences between cores and rims of Kilgore Tuff zircons are within the resolution of our method.

We recalculated previously published sanidine ^{40}Ar/^{39}Ar dates for the Kilgore Tuff (Morgan and McIntosh, 2005) employing the Fish Canyon Tuff sanidine standard calibration of Kuiper et al. (2008). This calibration was preferred on the basis of its demonstrated consistency with independent geochronometers for young rocks (e.g., Meyers et al., 2012; Rivera et al., 2013; Wotzlaw et al., 2013). The recalculated mean sanidine ^{40}Ar/^{39}Ar date is 4.510 ± 0.047 Ma, overlapping with all individual zircon ^{206}Pb/^{238}U dates from the Kilgore Tuff. If this sanidine ^{40}Ar/^{39}Ar date is taken as the eruption age of the Kilgore Tuff, then δ^{18}O-diverse zircons crystallized within several thousand years before eruption. This short time interval for reservoir assembly and magma storage is consistent with mineral diffusive time scales derived from oxygen isotopic heterogeneities in zircon and our estimates based on zircon microlite growth rates. The short duration of magma reservoir assembly recorded by Kilgore zircons is, however, in stark contrast to zircon records from long-lived magmatic systems such as the Fish Canyon Tuff (e.g., Wotzlaw et al., 2013), requiring significantly different reservoir assembly mechanisms and pre-eruption thermal histories.

The presence of two xenocrystic zircons (Fig. 2) that correspond in age to one of the previous eruptions at Heise that produced the Conant Creek Tuff, is additional evidence that magma generation was governed by remelting of related buried tuffs and subcaldera intrusions. This is also consistent with the homogeneity of zircons with respect to their Hf isotopic composition and their Th/U (Fig. DR3; Tables DR2 and DR3). Hafnium isotopic and chemical homogeneity of various subreservoirs requires long-term hybridization and homogenization of the subcaldera crust throughout the Heise caldera cycle. The homogeneous mixture of crustal and mantle-derived Hf and uniform Th/U in Kilgore zircons thus require a recycled origin of the Kilgore magma, and shallow crustal melting did not involve ultralow ε_{Hf} Archean crust, as found elsewhere in the Snake River Plain (Drew et al., 2013).

CAUSAL LINK BETWEEN BATCH ASSEMBLY AND ERUPTION?

Zircons that are indistinguishable in age, but highly diverse in δ^{18}O, suggest that the generation and subsequent amalgamation and mixing of isotopically distinct magma batches occurred within the resolution of our geochronology and shortly before eruption, as indicated by indistinguishable sanidine ^{40}Ar/^{39}Ar dates (Fig. 2). The merging of subreservoirs may have caused the system to evolve to a critical state that culminated in the eruption of the Kilgore Tuff. Eruptions occur when the overpressure in the magma reservoir is sufficiently high to overcome crustal yield strength. In smaller magmatic systems this can be caused by injections of new magma at reasonable rates. To trigger large-volume eruptions by magma recharge, extremely high magma injection rates would be required to significantly increase the pressure in the reservoir. Rather than super high rates of magma production and injection, we here advocate an eruption trigger mechanism that is the direct consequence of the reservoir assembly process.

Geophysical data from the Yellowstone and Toba volcanoes suggest that several laterally extensive magma reservoirs are present over a vertical distance of a few kilometers (Miller and Smith, 1999; Husen et al., 2004; Stankiewicz et al., 2010), and our data from the Kilgore Tuff suggest a similar pre-eruption reservoir configuration with several isolated subchambers. Magma in such reservoirs is less dense than the surrounding rock, generating buoyancy overpressure (Jellinek and DePaolo, 2003; Caricchi et al., 2014). Recently, Caricchi et al. (2014) and Malfait et al. (2014) demonstrated that buoyancy overpressure may be sufficient to trigger supereruptions. The maximum buoyancy overpressure at the roof of a magma chamber depends on the difference in density between magma and crust and on the vertical extent of the reservoir. Individual sill-like pools may not be buoyant enough to overcome crustal yield strength, and thus do not erupt. However, the connection of such pools (e.g., by thermal erosion/bulk assimilation or mechanical failure of intrareservoir crust; Fig. 3) located at different depths would lead to a rapid increase in buoyancy overpressure potentially sufficient to trigger eruption.

This study thus provides important geochronologic and isotopic evidence for a rapid mechanism of assembly of supervolcanic magma reservoirs in the shallow crust that may be causally linked to the eruption trigger, and provides an alternative model to slow-growing, mush-dominated systems that require hundreds of thousands of years to evolve to an eruptible state.

ACKNOWLEDGMENTS

This project was supported by the Swiss National Science Foundation, European Community FP7/2007-2013 grant 215458, and U.S. National Science Foundation grant EAR-CAREER-844772. We thank J.B. Lowenstern, B.S. Ellis, and an anonymous reviewer for constructive reviews.

REFERENCES CITED

Bindeman, I.N., and Valley, J.W., 2001, Low- δ18O rhyolites from Yellowstone: Magmatic evolution based on analyses of zircons and individual phenocrysts: Journal of Petrology, v. 42, p. 1491–1517, doi:10.1093/petrology/42.8.1491.

Bindeman, I.N., Watts, K.E., Schmitt, A.K., Morgan, L.A., and Shanks, P.W.C., 2007, Voluminous low-δ18O magmas in the late Miocene Heise volcanic field, Idaho: Implications for the fate of Yellowstone hotspot calderas: Geology, v. 35, p. 1019–1022, doi:10.1130/G24141A.1.

Bindeman, I.N., Fu, B., Kita, N., and Valley, J.W., 2008, Origin and evolution of Yellowstone silicic magmatism based on ion microprobe analysis of isotopically-zoned zircons: Journal of Petrology, v. 49, p. 163–193, doi:10.1093/petrology/egm075.

Caricchi, L., Annen, C., Blundy, J., Simpson, G., and Pinel, V., 2014, Frequency and magnitude of volcanic eruptions controlled by magma injection and buoyancy: Nature Geoscience, v. 7, p. 126–130, doi:10.1038/ngeo2041.

Cooper, G.F., Wilson, C.J.N., Millet, M.A., Baker, J.A., and Smith, E.G.C., 2012, Systematic tapping of independent magma chambers during the 1 Ma Kidnappers supereruption: Earth and Planetary Science Letters, v. 313–314, p. 23–33, doi:10.1016/j.epsl.2011.11.006.

Crowley, J.L., Schoene, B., and Bowring, S.A., 2007, U-Pb dating of zircon in the Bishop Tuff at the millennial scale: Geology, v. 35, p. 1123–1126, doi:10.1130/G24017A.1.

Drew, D.L., Bindeman, I.N., Watts, K., Schmitt, A.K., Fu, B., and McCurry, M., 2013, Crustal scale recycling in caldera complexes and rift zones of the Snake River Plain: O and Hf isotopic evidence in diverse zircons from low-δ18O rhyolites of the Picabo volcanic field, Idaho: Earth and Planetary Science Letters, v. 381, p. 63–77, doi:10.1016/j.epsl.2013.08.007.

Ellis, B.S., Bachmann, O., and Wolff, J.A., 2014, Cumulate fragments in silicic ignimbrites: The case of the Snake River Plain: Geology, v. 42, p. 431–434, doi:10.1130/G35399.1.

Husen, S., Smith, R.B., and Waite, G.P., 2004, Evidence for gas and magmatic sources beneath the Yellowstone volcanic field from seismic tomography imaging: Journal of Volcanology and Geothermal Research, v. 131, p. 397–410, doi:10.1016/S0377-0273(03)00416-5.

Jellinek, A.M., and DePaolo, D.J., 2003, A model for the origin of large silicic magma chambers: Precursors of caldera-forming eruptions: Bulletin of Volcanology, v. 65, p. 363–381, doi:10.1007/s00445-003-0277-y.

Kuiper, K.F., Deino, A., Hilgen, F.J., Krijgsman, W., Renne, P.R., and Wijbrans, J.R., 2008, Synchronizing rock clocks of Earth history: Science, v. 320, p. 500–504, doi:10.1126/science.1154339.

Lowenstern, J.B., Smith, R.B., and Hill, D.P., 2006, Monitoring super-volcanoes: Geophysical and geochemical signals at Yellowstone and other large caldera systems: Royal Society of London Philosophical Transactions, ser. A, v. 364, p. 2055–2072, doi:10.1098/rsta.2006.1813.

Malfait, W.J., Seifert, R., Petitgirard, S., Perrillat, J.P., Mezouar, M., Ota, T., Nakamura, E., Lerch, P., and Sanchez-Valle, C., 2014, Supervolcano eruptions driven by melt buoyancy in large silicic magma chambers: Nature Geoscience, v. 7, p. 122–125, doi:10.1038/ngeo2042.

Mason, B.G., Pyle, D.M., and Oppenheimer, C., 2004, The size and frequency of the largest explosive eruptions on Earth: Bulletin of Volcanology, v. 66, p. 735–748, doi:10.1007/s00445-004-0355-9.

Meyers, S.R., Siewert, S.E., Singer, B.S., Sageman, B.B., Condon, D.J., Obradovich, J.D., Jicha, B.R., and Sawyer, D.A., 2012, Intercalibration of radioisotopic and astrochronologic time scales for the Cenomanian-Turonian boundary interval, Western Interior Basin, USA: Geology, v. 40, p. 7–10, doi:10.1130/G32261.1.

Miller, D.S., and Smith, R.B., 1999, P and S velocity structure of the Yellowstone volcanic field from local earthquake and controlled-source tomography: Journal of Geophysical Research, v. 104, p. 15105–15121, doi:10.1029/1998JB900095.

Morgan, L.A., and McIntosh, W.C., 2005, Timing and development of the Heise volcanic field, Snake River Plain, Idaho, western USA: Geological Society of America Bulletin, v. 117, p. 288–306, doi:10.1130/B25519.1.

Peng, X., and Humphreys, E.D., 1998, Crustal velocity structure across the eastern Snake River Plain and the Yellowstone swell: Journal of Geophysical Research, v. 103, p. 7171–7186, doi:10.1029/97JB03615.

Pierce, K.L., and Morgan, L.A., 2009, Is the track of the Yellowstone hotspot driven by a deep mantle plume? Review of volcanism, faulting, and uplift in light of new data: Journal of Volcanology and Geothermal Research, v. 188, p. 1–25, doi:10.1016/j.jvolgeores.2009.07.009.

Rivera, T.A., Storey, M., Schmitz, M.D., and Crowley, J.L., 2013, Age intercalibration of $^{40}Ar/^{39}Ar$ sanidine and chemically distinct U/Pb zircon populations from the Alder Creek rhyolite quaternary geochronology standard: Chemical Geology, v. 345, p. 87–98, doi:10.1016/j.chemgeo.2013.02.021.

Schmandt, B., Dueker, K., Humphreys, E., and Hansen, S., 2012, Hot mantle upwelling across the 660 beneath Yellowstone: Earth and Planetary Science Letters, v. 331–332, p. 224–236, doi:10.1016/j.epsl.2012.03.025.

Self, S., and Blake, S., 2008, Consequences of explosive supereruptions: Elements, v. 4, p. 41–46, doi:10.2113/GSELEMENTS.4.1.41.

Shane, P., Nairn, I.A., Smith, V.C., Darragh, M., Beggs, K., and Cole, J.W., 2008, Silicic recharge of multiple rhyolite magmas by basaltic intrusion during the 22.6 ka Okareka eruption episode, New Zealand: Lithos, v. 103, p. 527–549, doi:10.1016/j.lithos.2007.11.002.

Simakin, A.G., and Bindeman, I.N., 2012, Remelting in caldera and rift environments and the genesis of hot, "recycled" rhyolites: Earth and Planetary Science Letters, v. 337–338, p. 224–235, doi:10.1016/j.epsl.2012.04.011.

Stankiewicz, J., Ryberg, T., Haberland, C., Fauzi, and Natawidjaja, D., 2010, Lake Toba volcano magma chamber imaged by ambient seismic noise tomography: Geophysical Research Letters, v. 37, L17306, doi:10.1029/2010GL044211.

Watts, K.E., Bindeman, I.N., and Schmitt, A.K., 2011, Large-volume rhyolite genesis in caldera complexes of the Snake River Plain: Insights from the Kilgore Tuff of the Heise Volcanic Field, Idaho, with comparison to Yellowstone and Bruneau-Jarbidge rhyolites: Journal of Petrology, v. 52, p. 857–890, doi:10.1093/petrology/egr005.

Wilson, C.J.N., and Hildreth, W., 1997, The Bishop Tuff: New insights from eruptive stratigraphy: Journal of Geology, v. 105, p. 407–440, doi:10.1086/515937.

Wotzlaw, J.F., Schaltegger, U., Frick, D.A., Dungan, M.A., Gerdes, A., and Günther, D., 2013, Tracking the evolution of large-volume silicic magma reservoirs from assembly to supereruption: Geology, v. 41, p. 867–870, doi:10.1130/G34366.1.

Manuscript received 11 June 2014
Revised manuscript received 25 June 2014
Manuscript accepted 28 June 2014

Printed in USA